THERMAL NON-EQUILIBRIUM EFFECTS IN RADICAL FARMING SCRAMJETS

Rolf M. Gehre*, Vincent Wheatley*, Russell R. Boyce*
***Centre for Hypersonics,**
The University of Queensland,
Brisbane, QLD 4072, Australia,
r.gehre@uq.edu.au

Keywords: *thermal non-equilibrium, hypersonic flow, scramjet, computational fluid dynamics*

Abstract

To analyze the effect of thermal non-equilibrium on radical farming scramjets, Reynolds-averaged Navier-Stokes (RANS) simulations have been performed. The investigation focuses on the potential combustion processes originating from hot regions within the combustor (hot pockets). To investigate thermal non-equilibrium effects independently from the injection method and the fuel type, a 5 species air model is used for the simulations and the effective temperature is employed as a qualitative measure for the combustion potential. The effect of shock-tunnel-testing is of particular interest. Therefore, a Mach 6 shock tunnel nozzle and a radical farming scramjet model have been simulated for an enthalpy condition of $4.17MJ/kg$*. Performing thermal equilibrium and non-equilibrium simulations for both the nozzle and scramjet, shows the effects of thermal non-equilibrium. For thermal equilibrium simulations, the effective temperatures in the hot pocket regions are higher than for thermal non-equilibrium simulations, indicating increased combustion potential for shock tunnel experiments.*

1 Introduction

To make space travel more affordable and efficient, an alternative transportation system needs to be developed. The research being undertaken at the University of Queensland (UQ) focuses on supersonic combustion ramjets (scramjets)[1]. The main advantage over rocket propulsion is that the oxidizer does not need to be carried on board, since the oxygen in the atmosphere is being used. Thus a higher specific impulse can be achieved. Unfortunately, this technology has one major drawback. As flight Mach number increases, it becomes difficult to overcome losses and generate net thrust.

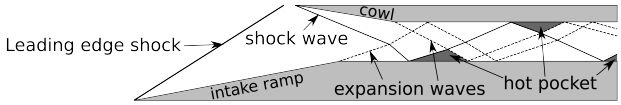

Fig. 1 : Schematic drawing of the *radical farming* scramjet used by Boyce et al. [4].

The *radical farming*[2, 3, 4] concept allows ignition and efficient combustion to be achieved with lower inlet compression, allowing losses to be reduced. This concept takes advantage of the flow/shock structure in the combustor. Regions of locally high temperatures known as *hot pockets* form within the combustor and initialize the combustion process by producing radicals as shown in figure 1. When the concentration of these radicals reaches a certain threshold, ignition occurs and the heat release process starts.

The main influencing factor for the ignition process (initiation reaction), assuming a perfectly mixed gas with an equivalence ratio $\phi = 1$, is the temperature. Thus, it is of great importance

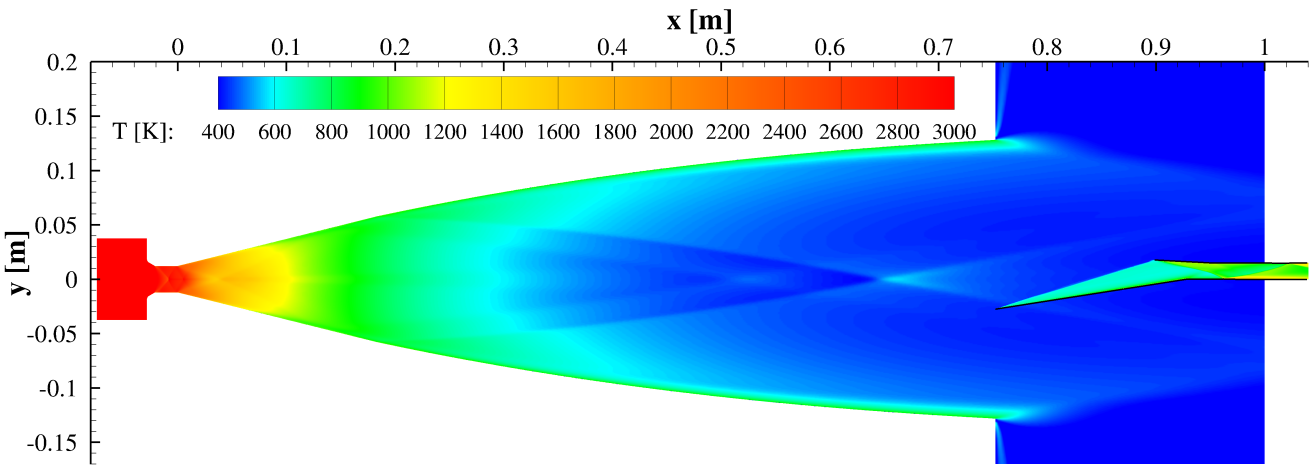

Fig. 2 : Translational-rotational temperature contour plot of the combined nozzle-scramjet arrangement.

to predict the correct temperature within the hot pockets. This paper focuses on the effect of thermal non-equilibrium within the scramjet. Especially, scramjet experiments in shock tunnels exhibit strong non-equilibrium effects at the nozzle exit and thus at the scramjet intake. Several computational fluid dynamic (CFD) simulations of the scramjet geometry shown in figure 4 have been undertaken to evaluate the importance of modeling thermal non-equilibrium and its effect on the temperatures within the engine.

2 Theory and numerical modeling

A polyatomic gas, e.g. oxygen or nitrogen, stores its internal energy in several modes; translational, rotational, vibrational and electronic. The electronic mode will be disregarded in further discussions, since it is not excited for the present conditions. The distribution of energy between these modes depends on the temperature of the gas and is referred to as *thermal equilibrium* when the characteristic temperatures T_t, T_r, T_v of each energy mode are equal. A sudden change of flow properties, e.g. due to shocks or rapid expansions, disrupts the equilibrium energy distribution and causes the characteristic temperatures to change, which results in $T_t \neq T_r \neq T_v$, called *thermal non-equilibrium*. Now, the disrupted energy modes relax towards equilibrium by exchanging energy via molecular collisions. Since only a few collisions are necessary for the translational and rotational temperatures to align, they can be considered to be in equilibrium ($T = T_t = T_r$) for flow conditions relevant for this paper. The relaxation process between the translational and vibrational modes takes much longer, which results in regions of non-equilibrium ($T \neq T_v$). The speed of the relaxation process can be calculated using the Landau-Teller relaxation model [5] coupled with the semi-empirical formulation of Millikan and White for the relaxation time [6, 7].

To model the thermal relaxation process an additional differential equation for the vibrational energy has to be solved, which increases the numerical cost. Additionally, it was assumed in the past that the temperature in the scramjet combustor is high enough to cause a fast relaxation process and hence result in thermal equilibrium. Thus equilibrium codes seemed adequate. But for radical farming scramjets the temperatures before ignition are relatively mild, which means that the non-equilibrium region can be quite extensive. Therefore, thermal non-equilibrium simulations are necessary to account for flow-field and flow-structure changes. The numerical code, US3D[8] is used here to simulate the scramjet flow, and solves the compressible Navier-Stoke-equations, which include thermal non-equilibrium terms for the two-temperature model. US3D employs a hybrid structured/unstructured cell-centered finite volume scheme.

Both the nozzle and scramjet flow are modeled in chemical non-equilibrium employing the finite rate, 5 species (N_2, O_2, NO, N and O) chemistry model for air which was proposed by Park [9]. Since the experimental test time is on the order of milliseconds, an isothermal wall with $T_{wall} = 300\,\mathrm{K}$ is assumed for all numerical simulations.

3 Flow conditions

All numerical simulations are based on the following experimental campaign: A Mach 6 nozzle used in the T3 reflected shock tunnel facility at the Australia National University [10] has been used to generate the inflow for the scramjet engine. The stagnation conditions are $h_0 = 4.17\,\mathrm{MJ/kg}$, $p_0 = 18.0\,\mathrm{MPa}$ and $T_0 = 3305\,\mathrm{K}$, which generate an equivalent flight Mach number of 9.5. The 2D scramjet model used by J. McGuire [4] to investigate the radical framing principle has been used to ensured that radical farming conditions are present.

First, the nozzle flow is simulated, employing the Reynolds-averaged Navier Stokes (RANS) equations, for two different conditions: (NE) Thermal non-equilibrium and (EQ) a forced equilibrium condition where the relaxation time $\tau \to 0$. The results of the numerical simulations are then extracted at the nozzle exit and used as inflow for the scramjet as shown in figure 2. The following three scramjet simulations have been carried out: (EQ-EQ) a thermal equilibrium scramjet simulation where the inflow is taken from the thermal equilibrium nozzle simulation, which is a common assumption; (EQ-NE) a thermal non-equilibrium scramjet simulation where the inflow is taken again from the thermal equilibrium nozzle simulation, which represents a flight test scenario; and (NE-NE) a thermal non-equilibrium scramjet simulation where the inflow is extracted from the thermal non-equilibrium nozzle simulation, which is representative of the shock-tunnel scenario.

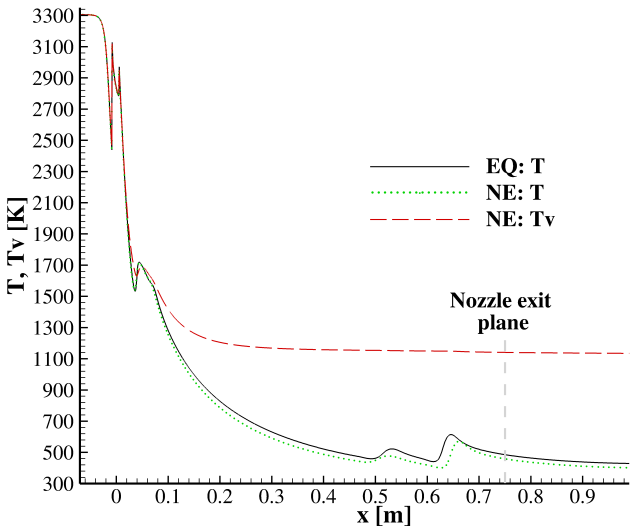

Fig. 3 : Translational-rotational and vibrational temperature distributions along the nozzle centerline.

4 Results

This section analyses the effect of thermal non-equilibrium on the flow conditions and structures developing in the nozzle and scramjet.

4.1 Nozzle

As mentioned in section 3, the nozzle flow is simulated in both thermal equilibrium and non-equilibrium. The resulting temperature distributions along the centerline are shown in Figure 3. It can be assumed that the nozzle stagnation region is in thermal equilibrium since the temperatures are high and the flow speed negligibly small. However, due to the rapid expansion through the nozzle, non-equilibrium effects become noticeable approximately 25 mm after the throat and lead to thermal freezing around 500 mm upstream of the nozzle exit. This leads to an approximate vibrational temperature at the nozzle exit centerline of 1140 K. The translational-rotational temperature measures 458 K, which is 27 K lower than the calculated translational-rotational temperature of the thermal equilibrium simulation. For the thermal non-equilibrium simulation, the nozzle exit Mach number at the centerline is 6.31, whereas the equilibrium simulation predicts a Mach num-

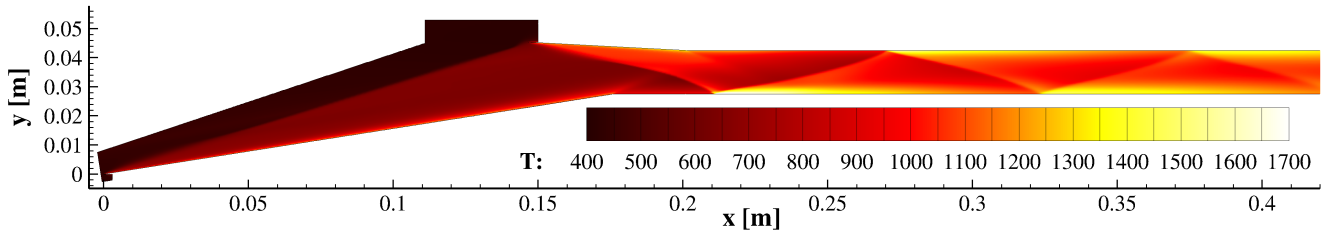

Fig. 4 : CFD result of the (NE-NE) simulation; the thick black lines indicate the scramjet boundaries.

ber of 6.03 . This difference results from changed translational-rotational nozzle exit temperatures and the fact that the compression waves deviate slightly between the thermal equilibrium and non-equilibrium simulations, which effects the nozzle outflow profile as well.

In conclusion, it can be noted that the general flow properties at the nozzle exit, e.g. translational-rotational temperature, Mach number, pressure, show only moderate differences due to the inclusion of thermal non-equilibrium effects. However, in the non-equilibrium case, the scramjet inflow will contain highly excited vibrational modes, which may have significant implications for ignition.

4.2 Scramjet

This subsection compares the three cases, EQ-EQ, EQ-NE and NE-NE, which are mentioned in section 3, with each other. It will be shown that the thermal non-equilibrium simulations of the scramjet produce similar results, even though the inflows had quite different thermal energy distributions, whereas the pure thermal equilibrium simulation deviates significantly from the thermal non-equilibrium simulations

To begin with the basic structure of the flow field within the scramjet is analyzed. This is shown in Figure 4, which displays the translational-rotational temperature distribution for the NE-NE case. It can be seen how the forebody shock is closely aligned with the inlet ramp, due to the hypersonic nature of the flow, and barely clears the tip of the cowl. Another shock originating from the cowl travels downwards to the lower combustor wall, while simultaneously expansion waves, originating from the corner where the inlet ramp transitions into the combustion camber, travel upwards to the upper combustor wall. These two dominant waves are reflected between the combustor walls as illustrated in Figure 1 and slowly decrease in strength with increasing distance along the combustor, as can be seen in Figure 4. The shock reflection at the combustor wall produces a very hot region immediately downstream, which is terminated by the impinging expansion waves further downstream. These hot regions (or pockets) are utilized in radical farming scramjets. Figure 4 visualizes these hot pockets. It is noticeable that the shape of the highest temperature regions differs from the ideal shaped hot pocket shown in Figure 1, due to the strong viscous dissipation effects within the boundary layer. However, the viscous hot pocket region is also terminated downstream of the shock impingement, due to the impinging expansion waves, which is characteristic of the radical farming engine concept. Furthermore, it becomes apparent that the first hot pocket at the lower combustor wall shows the largest temperature increase. The hot pockets further downstream show a milder temperature rise. To determine the effects of thermal non-equilibrium, the core flow, basically the inviscid part of the flow, is firstly analyzed. Afterwards the viscous regions, more specifically the hot pocket regions, are examined.

Figure 5 shows the temperature distributions for the EQ-EQ, EQ-NE and NE-NE cases. The temperatures are extracted along a streamline, which runs roughly through the middle of the combustor. The first two translational-rotational temperature rises in Figure 5 are due to the forebody and the cowl shock. The forebody shock

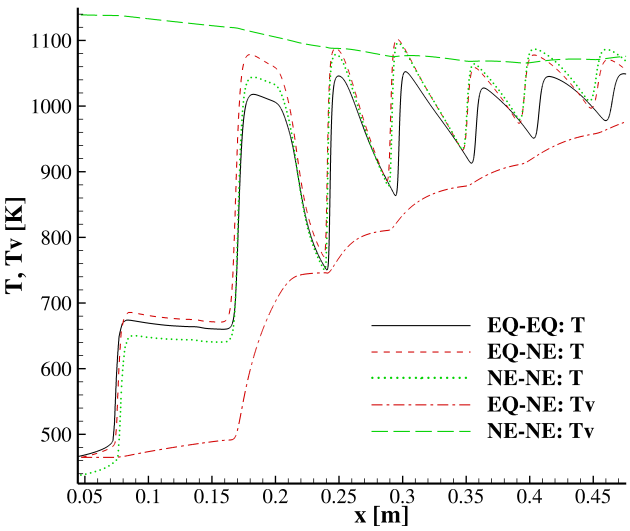

Fig. 5 : Temperature distributions for the EQ-EQ, EQ-NE and NE-NE cases within the scramjet along a streamline through the middle of the combustor.

locations for the EQ-EQ and EQ-NE cases are close to each other, whereas the shock location for the NE-NE case is shifted downstream, which is caused by a lower shock angle. This is explainable by a decreased ratio of specific heats, γ. In general, with increasing vibrational temperature γ decreases towards the limit of $\gamma = 1.286$, increasing the flow Mach number by decreasing the sound speed, which ultimately decreases the shock angle. Further downstream, at $x = 0.21\,\mathrm{m}$, a translational-rotational temperature drop is noted, which is caused by a dominant and an inferior expansion wave, which originate from the transition corners between the inlet ramp and cowl with the combustion chamber. From here on a periodic translational-rotational temperature increase and decrease is noticeable. It becomes apparent that the initially similar flow structures of the EQ-EQ and EQ-NE cases diverge with increasing streamwise distance, whereas the flow structures of the EQ-NE and NE-NE cases converge towards each other. In both thermal non-equilibrium simulations, the relatively slow response of the vibrational temperature to changes in the flow conditions is clearly visible. Downstream of the forebody shock, T_v relaxes towards equilibrium very gradually on the flow time scale. Downstream of the cowl and subsequent shocks, the decreased velocity and increased T and p of the flow allows the relaxation to proceed more rapidly. However, there is never sufficient time between waves for the flow to approach thermal equilibrium.

Additionally, the translational-rotational temperature inside the scramjet combustor is high, quickly approaching the vibrational temperature seen in the NE inflow, and generating sufficiently high vibrational excitation rates for the EQ-NE case that the local vibrational temperature, almost reaches the translational-rotational temperature. So, in both non-equilibrium scramjet simulations, EQ-NE and NE-NE, T_v tends towards T (although from opposite directions), and since only a small fraction of the total energy is stored in the vibrational mode, the two non-equilibrium cases quickly look very similar in structure. It should be mentioned that there is no specific curve for the vibrational temperature for case EQ-EQ since it is equal to the translational-rotational temperature. In summary, even though the EQ-NE and NE-NE cases started off with different inflow conditions, the translational-rotational temperature distributions further downstream are very similar. On the other hand, the temperature distribution of the EQ-EQ case diverges from the other two cases and results in decreased translational-rotational temperatures.

Next, the viscous part of the combustion chamber will be analyzed, which incorporates the hot pockets. The first hot pocket, located at the lower combustion chamber wall, will be used representatively for the other hot pockets. The highest temperatures are encountered in this hot pocket, thus it would act as an important initiator for combustion, since the initialization reactions that produce free chemical radicals are highly influenced by temperature.

Figure 6 shows the temperature distributions along a streamline, which is located approximately 0.15 mm above the lower intake and combustion chamber wall. Since a streamline through a two-dimensional domain contains only a frac-

tion of the original information, the magnitude of the temperature peaks in Figure 6 differ from those in the contour plot, but the general trends are represented correctly.

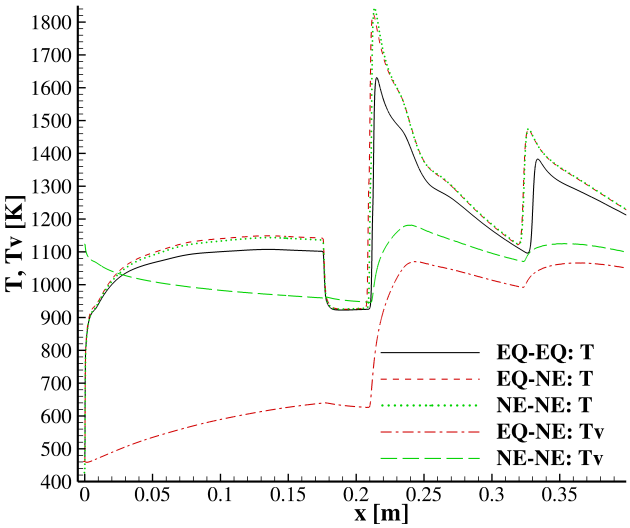

Fig. 6 : Temperature distributions for the EQ-EQ, EQ-NE and NE-NE cases within the scramjet along a streamline located approximately 0.15 mm above the lower scramjet wall.

The translational-rotational temperature rise right at the start of the flow domain ($x = 0.0m$) is due to the forebody shock. Since the streamline runs through the boundary layer of the inlet ramp, the temperature increases gradually due to viscous dissipation until a sudden translational-rotational temperature drop occurs at $x = 0.174$ m, which is caused by the expansion fan originating from the end of the ramp. Further downstream the translational-rotational temperature increases again due to the cowl shock impingement. From there on the translational-rotational temperature decreases and increases due to expansion and shock wave impingements as described for Figure 5. A similar flow structure to that seen in Figure 5 evolves. Of course the temperatures are much higher, as the kinetic energy has been dissipated in the boundary layer. Another effect that can not be seen in Figure 5 is the drop in the vibrational temperature for case NE-NE right from the start of the flow domain ($x = 0.0m$). This drop is caused by the boundary layer forcing the vibrational temperature towards the wall temperature, 300 K. Interestingly, the change in the vibrational temperature in the same region for case EQ-NE is chiefly caused by thermal relaxation. A mild influence of the boundary layer becomes apparent for the region between the expansion corner, $x = 0.174$ m, and the location of the first hot pocket, $x = 0.21$ m, due to a significant growth of the boundary layer.

So far local distributions of the temperatures have been analyzed to gain an understanding of the processes causing the temperature differences between non-equilibrium and equilibrium scramjet simulations. Since these distributions represent only local values, they may not be representative of the entire hot pocket, thus contour plots of the hot pocket are displayed in Figure 7.

From Figure 7, it is apparent that the general trend observed in the local temperature distributions agrees well with the contour plot. However, the maximum temperatures are different, resulting in higher temperature differences between the three cases. The maximum translational-rotational temperatures in the first hot pocket for the cases EQ-EQ, EQ-NE and NE-NE are $T = 1631$ K, $T = 1835$ K and $T = 1850$ K, respectively – the peak translational-rotational temperatures in the non-equilibrium scramjet simulations are approximately 200 K higher than the ones simulating equilibrium scramjet flow.

This temperature difference is caused by the redistribution of thermal energy. Since the vibrational temperature within the hot pockets for thermal non-equilibrium simulations (EQ-NE and NE-NE) is lower than that for equilibrium simulations (EQ-EQ), more energy is stored in the translational-rotational modes for non-equilibrium simulations, which results in increased translational-rotational temperatures. Furthermore, the specific wall heat flux is higher for the equilibrium simulations than for the non-equilibrium simulations due to boundary layer effects, which will not be discussed here. This causes the total energy near the wall to decrease, which in turn decreases the translational-rotational temperature. Additionally, the shock structure is different, which causes the tempera-

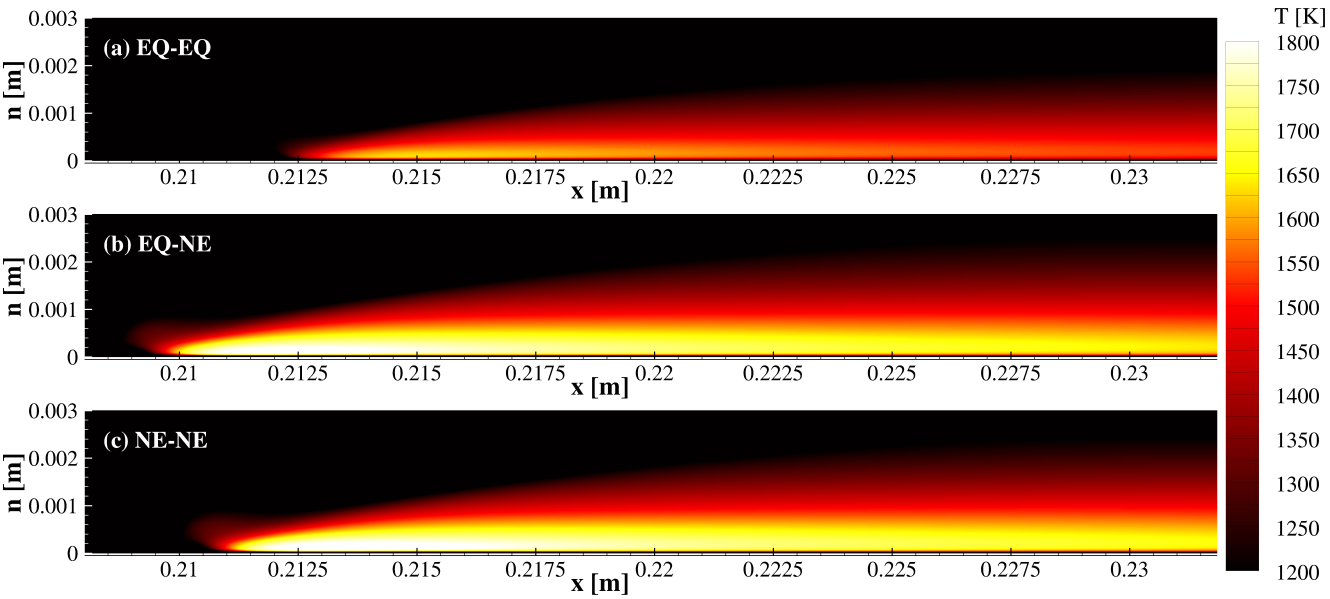

Fig. 7 : Detailed temperature of the hot pocket for the cases (NE-NE), (EQ-NE) and (EQ-EQ).

ture increase over shocks to be different. Moreover, the shock induced pressure increases are different, causing slightly different turning angles of the flow after shock-shock or shock-expansion wave interactions, which in turn cause different downstream shock angles, structure and strength. All these factors contribute to the observed temperature difference in the hot pocket, where the thermal energy distribution is the driving factor.

The second hot pocket on the upper wall of the combustion chamber, not displayed in this paper, exhibits a similar behavior with regard to the thermal non-equilibrium effect, but lower translational-rotational temperatures and temperature differences are encountered, due to the weaker shock impingement. Nevertheless, a general trend due to simulating thermal non-equilibrium can be observed.

5 Discussion

Thus far the effects of modeling thermal non-equilibrium on the translational-rotational and vibrational temperature distributions have been analyzed. Both temperatures influence the combustion process and thus have implications for the efficiency of the scramjet. The vibrational temperature particularly effects the initialization stage of combustion, which is meant to occur within the hot pockets and create enough radicals for combustion to commence further downstream. The rate of dissociation or radical production of a certain species increases with increasing vibrational temperature for a constant translational-rotational temperature. Consequently, the thermal and chemical state of a gas are coupled. To simulate this coupling, several models have been developed. A comparison of these models can be found in daSilva et al. [11]. Often Park's two temperature model [12] is employed to calculate an effective temperature:

$$T_{eff} = T^q T_v^{1-q} \ , \tag{1}$$

which is then used to determine the dissociation rates. The literature gives two values for q; 0.5 [13] and 0.7 [14]. For expanding flows, resulting in $T < T_v$, it is recommended to use $q = 0.5$ and for compressive flows, $T > T_v$, choosing $q = 0.7$ is advised according to daSilva et al. [11]. To smoothly transition between these two values the following equation for q;

$$q = \alpha - \beta \left(\frac{T_v}{T} \right) \ , \tag{2}$$

with $\alpha = 0.9$ and $\beta = 0.3$, is given by Hansen [15]. This equation has weaknesses for $T < T_v$, but since $T > T_v$ for the regions of interest here,

the hot pockets, equation 1 in combination with equation 2 is expected to produce reasonable results. Although this two-temperature model gives only an approximate estimate of the non-equilibrium impact on the dissociation rates, it nevertheless enables the impact of thermal non-equilibrium on scramjet combustion to be assessed.

The effective temperature T_{eff}, which characterizes the dissociation process and hence the rate of radical production, is highly correlated with the efficiency and ignition length of the combustion process. Employing the above two-temperature model to the flow through the scramjet geometry considered here results in the effective temperature distributions shown in Figure 8. This diagram is identical to Figure 6, except that the translational-rotational and vibrational temperatures have been replaced by the effective temperature.

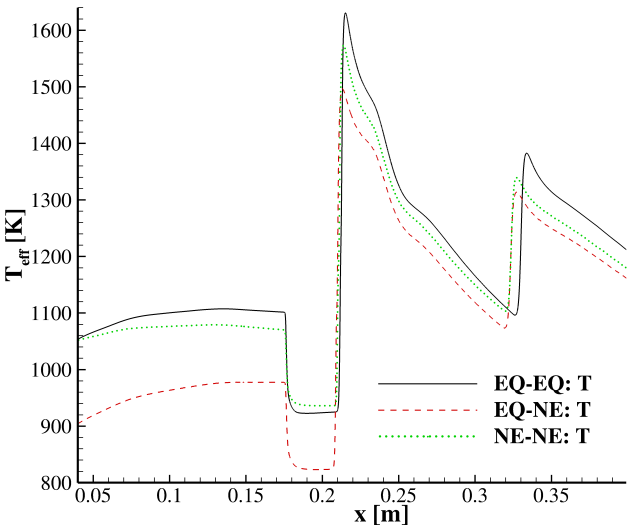

Fig. 8 : Effective temperature distribution of case EQ-EQ, EQ-NE and NE-NE with in the scramjet along a streamline located approximately 0.15 mm above the lower scramjet wall.

The result is quite surprising since all previously mentioned trends in translational-rotational temperature, which represents the majority of thermal energy, seem to be reversed. Firstly, the effective temperature distribution of the EQ-NE and NE-NE cases are not similar anymore. Secondly, the effective temperature of case EQ-EQ rises above those for the two thermal non-equilibrium cases. In retrospect, subsection 4.2 identified the thermal energy distribution as the main cause for the large translational-rotational temperature difference. However, the inverse trend for the effective temperature is explainable since the ratio of $\frac{T}{T_v}$, caused by the ratio of the thermal energies $\frac{E_t}{E_v}$, differs significantly from the relative weight of T and T_v used in the two-temperature model.

The maximum effective temperature within the first hot pocket for the EQ-EQ, EQ-NE and NE-NE cases are $T = 1631\,\mathrm{K}$, $T = 1499\,\mathrm{K}$ and $T = 1574\,\mathrm{K}$, respectively. This means that EQ-EQ simulations predict T_{eff} to be approximately 60 K higher than the NE-NE case and 130 K higher than the EQ-NE case. Consequently, modeling the scramjet flow to be in thermal equilibrium leads to faster dissociation rates and thus to more radicals produced, which start and accelerate the global combustion process. Furthermore, extrapolating combustion results from shock tunnel tests (NE-NE) to flight tests (EQ-NE), disregarding the different wall conditions, should be performed cautiously since the combustion behavior for shock tunnel tests is better due to a higher effective temperature.

Finally, it should be noted that although the effective temperature differences seem small, the reaction rates depend exponentially on T_{eff} and radical farming scramjets are often designed to operate close to the minimum compression, where combustion will be achieved through the shock induction process. Therefore, changes in T_{eff} and hence modeling thermal non-equilibrium can have significant impact on the predicted performance of radical farming engines.

6 Conclusion

This study shows that thermal non-equilibrium effects have a noticeable influence on the flow physics in radical farming scramjets. Firstly, the shock structures within the scramjet are similar for thermal non-equilibrium simulations (EQ-NE, NE-NE) and diverge from those modeling

purely thermal equilibrium (EQ-EQ). Secondly, the translational-rotational temperatures in the hot pockets are lower for thermal equilibrium simulations (EQ-EQ). However, the behavior of the effective temperature, used as a measure for combustion potential, is reversed indicating enhanced combustion for thermal equilibrium simulations. The simulation representing a flight condition (EQ-NE) shows the lowest effective temperatures in the hot pockets, whereas effective temperatures for the shock-tunnel-equivalent condition (NE-NE) lie between the two afore mentioned ones. Thus, it can be concluded that modeling thermal non-equilibrium increases the accuracy of the simulation and that thermal non-equilibrium inflow has the potential to enhance the combustion process in radical farming scramjets.

Acknowledgments

The authors would like to thank Professor Graham Candler's research group for providing the CFD research code. The research is funded by the Australian Space Research Program. This work was supported by an award under the Merit Allocation Scheme on the NCI National Facility at the ANU.

References

[1] W. H. Heiser and D. T. Pratt. *Hypersonic Airbreathing Propulsion*. AIAA Education Series, 1994.

[2] J. Odam and A. Paull. Radical farming in scramjets. In *Notes on Numerical Fluid Mechanics and Multidisciplinary Design*, volume 69, pages 276–283. Sringer, Berlin, 2008.

[3] J. R. McGuire, R. R. Boyce, and N. R. Mudford. Radical farm ignition processes in two-dimensional supersonic combustion. *Journal of Propulsion and Power*, 24(6):1248–1257, 2008.

[4] R. Boyce, N. Mudford, and J. McGuire. Ohplif visualisation of radical farming supersonic combustion flows. *Shock Waves*, 22:9–21, 2012.

[5] L. Landau and E. Teller. Zur theorie der schalldispersion. *Phys. Z. Sowjet.*, 10(1):34–43, 1936.

[6] R. C. Millikan and D. R. White. Systematics of vibrational relaxation. *J. Chem. Phys.*, 39(12):3209–3213, 1963.

[7] R. M. Gehre, V. Wheatley, and R. R. Boyce. Revised model coefficients for vibrational relaxation in a nitrogen-oxygen gas mixture. Technical report, Shock Waves (accepted for publication), June, 15th 2012.

[8] I. Nompelis, T. W. Drayna, and G. V. Candler. Development of a hybrid unstructured implicit solver for the simulation of reacting flows over complex geometries. In 34th *AIAA Fluid Dynamics Conference*, AIAA-2004-2227, Portland, 2004.

[9] C. Park. *Nonequilibrium Hypersonic Aerothermodynamics*. Wiley, New York, 1989.

[10] R. J. Stalker. Development of a hypervelocity wind tunnel. *The Aeronautical Journal*, 76:374–384, 1972.

[11] M. Lino da Silva, V. Guerra, and J. Loureiro. Two-temperature models for nitrogen dissociation. *Chemical Physics*, 342(1-3):275–287, 2007.

[12] Chul Park. Assessment of two-temperature kinetic model for ionizing air. *Journal of Thermophysics and Heat Transfer*, 3(3):233–244, 1989.

[13] C. Park. Assessment of a two-temperature kinetic model for dissociating and weakly ionizing nitrogen. *Journal of Thermophysics and Heat Transfer*, 1988.

[14] C. Park S. P. Sharma, W. M. Huo. Rate parameters for coupled vibration-dissociation in a generalized ssh approximation. *Journal of Thermophysics and Heat Transfer*, 1992.

[15] C.Frederick Hansen. Vibrational nonequilibrium effects on diatomic dissociation rates. *AIAA journal*, 31(11):2047–2051, 1993.

Copyright Statement

The authors confirm that they, and/or their company or organization, hold copyright on all of the original material included in this paper. The authors also confirm that they have obtained permission, from the copyright holder of any third party material included in this paper, to publish it as part of their paper. The authors confirm that they give permission, or have obtained permission from the copyright holder of this paper, for the publication and distribution of this paper as part of the ICAS2012 proceedings or as individual off-prints from the proceedings.